QUANTUM MECHANICAL INVESTIGATION OF CO OXIDATION CONDUCTED ON AUTOMOTIVE EXHAUST EMISSION CATALYSTS CONTAINING LA AND PD/LA ON CERIA-ZIRCONIA

A THESIS SUBMITTED TO
THE GRADUATE SCHOOL OF NATURAL AND APPLIED SCIENCES
OF
MIDDLE EAST TECHNICAL UNIVERSITY

BY

YASEMİN KAYA

IN PARTIAL FULFILLMENT OF THE REQUIREMENTS
FOR
THE DEGREE OF MASTER OF SCIENCE
IN
CHEMICAL ENGINEERING

JANUARY 2016

Approval of the thesis:

QUANTUM MECHANICAL INVESTIGATION OF CO OXIDATION CONDUCTED ON AUTOMOTIVE EXHAUST EMISSION CATALYSTS CONTAINING LA AND PD/LA ON CERIA-ZIRCONIA

submitted by **YASEMİN KAYA** in partial fulfillment of the requirements for the degree of **Master of Science in Chemical Engineering Department, Middle East Technical University** by,

Prof. Dr. Gülbin Dural _____
Dean, Graduate School of **Natural and Applied Sciences**

Prof. Dr. Halil Kalıpçılar _____
Head of Department, **Chemical Engineering**

Prof. Dr. Işık Önal _____
Supervisor, **Chemical Engineering Dept., METU**

Examining Committee Members:

Prof. Dr. İnci Eroğlu _____
Chemical Engineering Dept., METU

Prof. Dr. Işık Önal _____
Chemical Engineering Dept., METU

Assoc. Prof. Dr. Mehmet Ferdi Fellah _____
Chemical Engineering Dept., BTU

Assoc. Prof. Dr. Görkem Külah _____
Chemical Engineering Dept., METU

Assist. Prof. Dr. Erhan Bat _____
Chemical Engineering Dept., METU

Date: 26.01.2016

I hereby declare that all information in this document has been obtained and presented in accordance with academic rules and ethical conduct. I also declare that, as required by these rules and conduct, I have fully cited and referenced all material and results that are not original to this work.

Name, Last name : Yasemin Kaya

Signature :

ABSTRACT

QUANTUM MECHANICAL INVESTIGATION OF CO OXIDATION CONDUCTED ON AUTOMOTIVE EXHAUST EMISSION CATALYSTS CONTAINING LA AND PD/LA ON CERIA-ZIRCONIA

Kaya, Yasemin

M.Sc., Department of Chemical Engineering
Supervisor: Prof. Dr. Işık Önal

January 2016, 55 pages

In this study, Three Way Catalyst (TWC) is investigated via Density Functional Theory (DFT) methods. DFT techniques are implemented by Vienna Ab Initio Simulation Package (VASP). Atomic lanthanum substituted and both palladium and lanthanum substituted CZO (110) surfaces are investigated for their catalytic activity in terms of carbon monoxide oxidation. Relative energy profiles for CO reaction mechanisms on these surfaces are obtained and activation barriers of reaction steps are analyzed by using CI-NEB method. It is observed that Oxygen Storage Capacity (OSC) of CZO is remarkably enhanced by the introduction of lanthanum to CZO and Pd-CZO structure. The catalytic activity on La-doped surface in terms of CO oxidation is found as energetically more favorable

compared to Pd+La doped surface since there is no activation barrier for the reaction steps carried out on this surface.

Keywords: Three Way Catalytic Converters, Ceria-Zirconia, Carbon Monoxide Oxidation, Density Functional Theory, Computational Chemistry

ÖZ

LA VE PD/LA İÇEREN SERYUM-ZİRKONYUM OKSİT OTOMOTİV KATALİZÖRLERİ ÜZERİNDE CO OKSİDASYONUNUN KUANTUM MEKANİKSEL ÇALIŞMASI

Kaya, Yasemin

Yüksek Lisans, Kimya Mühendisliği Bölümü
Tez Yöneticisi: Prof. Dr. Işık Önal

Ocak 2016, 55 sayfa

Bu çalışmada, Üç Yollu Katalizör (TWC) Yoğunluk Fonksiyonel Teorisi (DFT) yöntemi kullanılarak incelenmiştir. DFT teknikleri Viyana Ab İnitio Simülasyon Paketi (VASP) yolu ile uygulanmıştır. Atomik lantan ve paladyum ile lantan birlikte yerleştirilmiş seryum-zirkonyum oksit (CZO) (110) yüzeylerin, karbon monoksit oksidasyonu açısından katalitik aktivitesi incelenmiştir. CO oksidasyon reaksiyon mekanizması için göreli enerji profilleri elde edilerek, aktivasyon engelleri CI-NEB yöntemi kullanılarak analiz edilmiştir. CZO ve Pd-CZO yüzeylerinin oksijen depolama kapasitesinin La metalinin yüzeye yerleştirilmesi ile dikkate değer bir artış gösterdiği gözlemlenmiştir. La yerleştirilmiş CZO yüzeyde gerçekleştirilen CO oksidasyonunun, reaksiyon basamaklarının

aktivasyon engeli içermemesi nedeni ile Pd+La içeren yüzeye göre enerji bakımından daha avantajlı olduğu bulunmuştur.

Anahtar Kelimeler: Üç Yollu Katalitik Konvertör, Seryum-Zirkonyum Oksit, Karbon Monoksit Oksidasyonu, Yoğunluk Fonksiyoneli Teorisi, Hesaplamalı Kimya

To My Family,
For your endless support and love

ACKNOWLEDGEMENTS

I wish to offer my sincere thanks and appreciation to my supervisor Prof. Dr. Işık Önal for his precious help, invaluable suggestions, continuous support, guidance, criticisms, encouragements and patience throughout this study.

I would like to thank my former and present colleagues Aylin Civan and İlker Tezsevin for their invaluable help and friendship throughout this study. I am also thankful to the present and past members of our research group, Dr. Derya Düzenli, Özgen Yalçın, Özlem Yönder, and Miray Gülbiter.

I would like to thank Fatma Şahin and Elif İrem Şenyurt for their friendship and all the times we spent together.

Sincerest thanks to my parents Ali and Gönül Kaya for supporting and believing in me all the way through my academic life.

TABLE OF CONTENTS

LIST OF TABLES

TABLES

LIST OF FIGURES

FIGURES

LIST OF ABBREVATIONS

A/F	Air to Fuel Ratio
CZO	Cerium Zirconium Oxide
DFT	Density Functional Theory
HC	Hydrocarbon
NOx	Nitrogen Oxides
OSC	Oxygen Storage Capacity
TWC	Three Way Catalyst

CHAPTER 1

INTRODUCTION

1.1. General Information

Exhaust emissions generated by gasoline motor vehicles are one of the main sources of air pollution, particularly in urban areas. In a perfect engine, all fuel reacts with air and is converted to water and carbon dioxide. Nitrogen in the air would remain unaffected. In reality, the complete combustion of fuel does not occur in the engine, and therefore carbon monoxide is produced besides unburned hydrocarbons. Additionally, due to high combustion temperatures, the radical reactions of nitrogen and oxygen produce several types of nitrogen oxides (Heck & Farrauto, 2001).

Three main components of exhaust gas are carbon monoxide, CO, partially burned or unburned hydrocarbons, HCs, nitrogen oxides, NOx, especially NO. Besides these components, hydrogen, H_2, water, H_2O, carbon dioxide, CO_2, oxygen, O_2, and nitrogen left, N_2 etc. are also exhaled by a typical gasoline engine. The composition of exhaust gas by volume percent of 0.5% CO, 350 ppmv HC, 900 ppmv NOx, and rest is given in Table 1.1. Among these components, main toxic pollutants are HC, CO and NOx.

Table 1.1 The main composition of exhaust gas for gasoline engines (Heck and Farrauto, 2001)

Component	Concentration
CO	0.5 vol.%
HC	350 ppmv
NOx	900ppmv
H_2	0.17 vol.%
H_2O	10 vol.%
CO_2	10 vol. %
O_2	0.5 vol.%

In order to protect the human health and environment, these pollutants have been restricted in the exhaust gas according to some regulations. In Europa, Euro Emission Standards are applied; other countries have also their regulations (i.e. in USA, EPA). Table 1.2 shows EU emission standards for passenger cars (a), and limitations by historical aspect in California (b).

Table 1.2 (a) Emission Standards in the World, (b) Californian emission limits (Twigg, 2011).

Stage	Date	CO	HC	HC+NOx	NOx	PM
		g/km				
Compression Ignition (Diesel)						
Euro 1†	1992.07	2.72 (3.16)	-	0.97 (1.13)	-	0.14 (0.18)
Euro 2, IDI	1996.01	1.0	-	0.7	-	0.08
Euro 2, DI	1996.01[a]	1.0	-	0.9	-	0.10
Euro 3	2000.01	0.64	-	0.56	0.50	0.05
Euro 4	2005.01	0.50	-	0.30	0.25	0.025
Euro 5a	2009.09[b]	0.50	-	0.23	0.18	0.005[f]
Euro 5b	2011.09[c]	0.50	-	0.23	0.18	0.005[f]
Euro 6	2014.09	0.50	-	0.17	0.08	0.005[f]
Positive Ignition (Gasoline)						
Euro 1†	1992.07	2.72 (3.16)	-	0.97 (1.13)	-	-
Euro 2	1996.01	2.2	-	0.5	-	-
Euro 3	2000.01	2.30	0.20	-	0.15	-
Euro 4	2005.01	1.0	0.10	-	0.08	-
Euro 5	2009.09[b]	1.0	0.10[d]	-	0.06	0.005[e,f]
Euro 6	2014.09	1.0	0.10[d]	-	0.06	0.005[e,f]

(a)

Table 1.2 Cont.d

Year	Category	Emissions (g mile^{-1}, FTP Test)			
		HC	CO	NOx	PM
1993	–	0.25[a]	3.40	0.40	–
1994	Tier 1	0.25[b]	3.40	0.40	–
2003	Tier 1	0.25[c]	3.40	0.40	–
2004	$TLEV_1$[d]	0.125	3.40	0.40	0.08
	LEV_2[e, f]	0.075	3.40	0.05	0.01
2005	LEV_1[d]	0.075	3.40	0.40	0.08
	$ULEV_2$[e, f]	0.040	1.70	0.05	0.01
2006	$ULEV_1$[d]	0.040	1.70	0.20	0.04
	$SULEV_2$[e, f, g]	0.010	1.0	0.02	0.01
2007	ZEV_1	0	0	0	0
	ZEV_2	0	0	0	0

(b)

In order to reduce the pollutants from exhaust gas, catalytic converters have been developed since 1974. Now, the catalytic converters are widely used for the control of the exhaust emissions of the gasoline vehicles by converting the harmful by-products CO, NOx, and HC to harmless compounds of H_2O, CO_2, and O_2 (Papavasiliou et al., 2009).

1.2. Three Way Catalyst

To control emission from gasoline vehicles, three way catalysts (TWC) are the main technology. The TWCs typically consist of;

1. a cordierite ($2MgO.2Al_2O_3.5SiO_2$) or metal honeycomb monolith in a stainless steel container,
2. a washcoat with high surface area (alumina),
3. oxygen storage materials (CeO_2-ZrO_2) coated on monolith,
4. the nobel metals such as Pt, Pd, and Rh acting as active phases, and
5. metal oxide as stabilizers and promoters. (Shim et al. 2011; Lucena et al. 1999; Kaspar et al. 2003)

The configuration of typical TWC is given in Figure 1.1. The composition of a TWC has varied by years depending on the design parameters and cost of the metals used in the active phase.

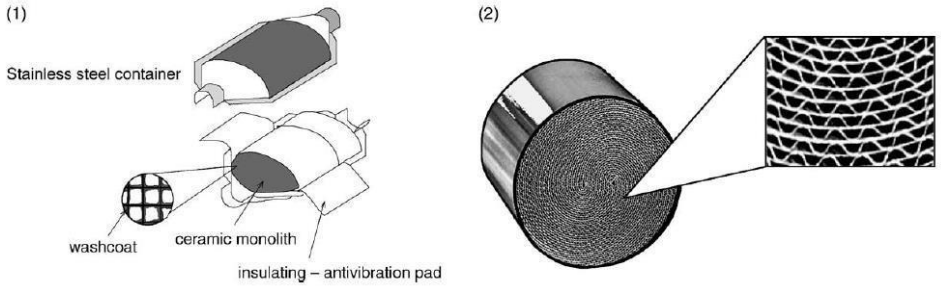

Figure 1.1 A diagram of a typical catalytic converter (1), and a metallic honeycomb (2) (Kaspar, 2003)

The main components of modern TWC are alumina as washcoat (support), ceria-zirconia, precious group metals (Pt,Pd, Rh) as active phases, various oxides as stabilizers of alumina surface area, activity promoters, selectivity promoters such as iron, manganese, calcium, lanthanum, neodymium, and zirconium (Twigg, 2011a).

Three way catalysts includes a lambda or oxygen sensor (λ) to adjust air to fuel ratio on gasoline engines and operate in a close loop system. The reduction and oxidation reactions over TWC should be carried out simultaneously for three main pollutants of CO and HCs and NOx. In this process, CO and HCs are oxidized to CO_2 and H_2O while NOx are reduced to N_2 (Kaspar, 2003). Main reactions taking place in TWC can be described as the equations given in Table 1.3. In this table, the desired products are given, H_2O, CO_2 and N_2. To obtain these products over the automotive catalyst, the high selectivity of the catalyst is required, because some other toxic compounds can be produces such as aldehydes and ammonia.

Table 1. 3 The main reactions in TWC (Wang et al., 2015)

Oxidation reactions:
$C_mH_n + O_2 \rightarrow CO_2\,(CO) + H_2O$
$CO + O_2 \rightarrow CO_2$
$H_2 + O_2 \rightarrow H_2O$
NO reduction reactions:
$NO \rightarrow N_2\,(N_2O, NH_3) + H_2O + CO_2$
$CO + NO \rightarrow CO_2 + N_2\,(N_2O)$
$H_2 + NO \rightarrow N_2\,(N_2O, NH_3) + H_2O$
Hydrogen production reactions:
$CO + H_2O \rightarrow CO_2 + H_2$
$C_mH_n + H_2O \rightarrow CO_2 + H_2$

1.3. Air to Fuel Ratio, A/F

Air-to-Fuel ratio (A/F) is an important parameter in combustion process. Stoichiometric value of A/F ratio is 14.7, and only at this value complete conversion of pollutants can take place and appropriate amount of oxidizing and reducing agents present in the exhaust gas (Kaspar et al., 2003). In the case of under the stoichiometric ratio, the fuel is rich, in other words oxygen amount is insufficient. As a result, the complete oxidation of CO and HCs does not carry out under stoichiometric ratio due to lack of oxygen. In the lean mode, contrarily, oxygen content in the exhaust is too high, which causes low NOx conversion (Gandhi et al., 1976). TWC response to the air/fuel ratio in a typical operation condition is given in Figure 1.1 (Heck, Farrauto, 2001).

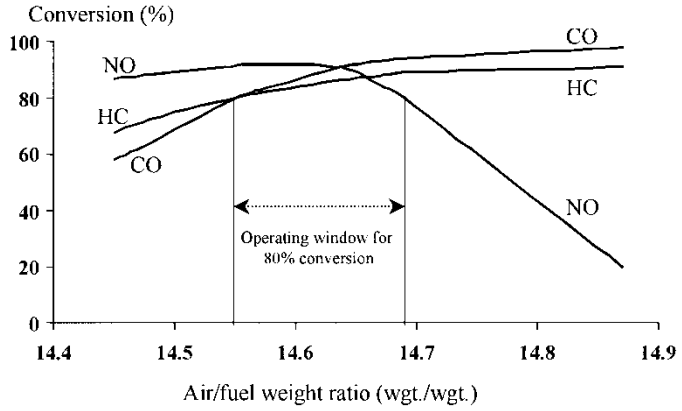

Figure 1.2 TWC efficiency for CO, HC and NOx conversions determined by engine air to fuel ratio.

Variations between fuel rich and fuel poor (lean burn) conditions cause a decrease of catalyst performance, since TWSs achieve the simultaneous conversions of CO, HC, NO*x* at only the stoichiometric air to fuel point. This phenomenon is due to the fact that Al_2O_3 do not store and release oxygen under exhaust gas converter conditions. In the beginnings of 1980s, CeO_2 was found to be promising as oxygen storage material (Kaspar et al., 1999).

CeO_2 improves the dispersion of noble metal, increases the thermal stability of alumina, promotes CO oxidation by using lattice oxygen, and has high oxygen storage capacity by storing and releasing oxygen under lean and rich conditions, respectively (Kaspar et al., 2003).

It is clear that CeO_2 in the support layer improves the performance of TWC by virtue of its high oxygen storage capacity (Kim, 1982).

However pure ceria has weak thermal stability at high exhaust gas temperatures, it has been gradually changed by the CeO_2-ZrO_2 mixed oxides in the TWCs starting from 1995. CeO_2 content in CeO_2-ZrO_2 mixture is an important parameter for thermal stability and OSC of the catalyst. Figure 1.3 shows the BET surface area and DOSC as a function of CeO_2 mole percent in CZO. As shown in Figure

1.3, the optimum composition for the most effective TWC performance is around 60-70 % mol CeO_2 compositions (Kaspar et al., 2003).

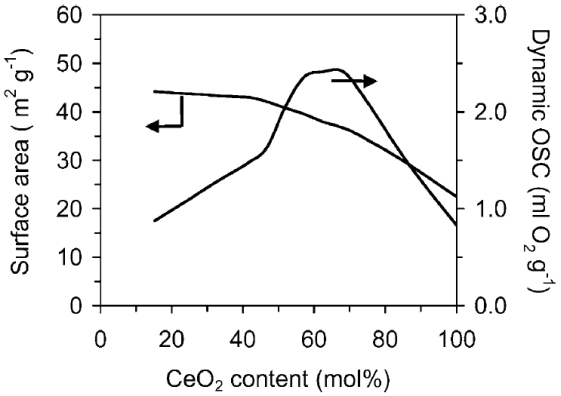

Figure 1.3 Effect of CeO_2 content on the surface area stability and dynamic oxygen storage capacity (at 400 °C) of CZO after calcination.

The deactivation starts with the increasing temperature, especially after 800°C. High temperature causes sintering, therefore, surface area of the catalyst and OSC decreases (Shelef et al., 2002). The solution to this problem is the incorporation of ZrO_2 into the CeO_2 lattice. It has been proved that CeO_2 is prevented effectively from sintering (Martinez et al., 2001).

1.4. Catalyst Deactivation

TWCs lose their catalytic properties due to the thermal aging and poisoning. High operating temperature causes sintering resulting in loss of redox property of catalyst, metal loss, alloy of noble metal and metal support (Granados et al., 2005; Fornasiero et al., 2000). Pb, S, P or other elements may cause poisoning of the catalyst. Coke formation and support pore structure blockage are also the other cases to cause the catalyst deactivation (Lassi, et al. 2004).

1.5. Computational Chemistry

Computational chemistry is a theoretical approach in solving chemical problems with the help of computers. Computational methods in chemistry has become a useful tool to solve complex problems so that researchers can make predictions before an experimental effort. Thus, it helps researcher save time and money. Theory of computational chemistry is based on quantum mechanics, classical mechanics, statistical physics, and thermodynamics.

With the increasing computer power, parallel and grid computing utilities, and successful numerical techniques, different computations have been efficiently conducted for chemical and biological modeling. Some of these models are molecular energies of molecules and structures geometry optimization, bond energies, reaction energies, reaction pathway, transition states structures and energies, all thermodynamic properties, vibrational frequencies, atomic charges, electrostatic potential, magnetic properties and so on (Ramanchandran, Deepa, & Namboori, 2008). However, computational methods give approximate results with desired degree of accuracy (Jensen, 2007).

Computational methods can be classified as ab initio methods, semi empirical calculations, molecular mechanics, molecular dynamics, and density functional theory (DFT) methods. Choosing a particular computation method depends on the size of the system, the desired accuracy and the computational facilities available. For example, for large systems such as proteins can be solved by using classical mechanics approach called molecular mechanics. In semi-empirical methods, parameter sets are based on experimental measurements. However, many molecules such as transition metals does not have sufficiently good parameter and cannot be treated by these methods with good accuracy.

Ab initio methods use approximation techniques to calculate the wave functions directly instead of assuming experimental parameters. These methods such as Hartree-Fock methods can be accurate, but computationally very expensive.

The last approach in computational chemistry is density functional theory (DFT). The computational cost is scaled with the N^3 in DFT methods while N^4 in Ab initio methods (N=number of basis set). Therefore, DFT is the most cost effective method with desired accuracy. DFT methods also account for the electron correlation; which is neglected in Ab initio methods. Electron correlation is defined as the difference between the Hartree-Fock energy and the exact solution of Schrödinger equation. Additionally, many structures such as transition metals can be treated well compared to other methods. As a result, DFT method is the most accurate and cost effective method for computational chemistry (Ramanchandran, Deepa, & Namboori, 2008). The energy accuracy of the method is between 10 and 40 kj/mol (van Santen and Sautet, 2008). Therefore, this research study is based on Density functional Theory.

The derivation of DFT method starts with the Schrödinger equation and based on two theorems of Hohenberg and Kohn (Parr and Yang, 1989). According to Hohenberg-Kohn theorems, the electronic energy of a system can be modelled by its electron density. The development of DFT is given by the following part.

1.5.1. Schrödinger Equation

Since probability density of micro-particles or atoms behaves wave-like it needs a differential equation which describes it, such as a wave function. This equation was developed by Erwin Schrödinger. The ground state energy of a collection of atoms may be computed by the time independent, nonrelativistic, Born-Oppenheimer approximation (1927) (the nuclei are kept fixed) form of Schrödinger Equation, which is;

$$\widehat{H}\Psi_i(r_1, r_2, \dots., r_N) = E\Psi_i(r_1, r_2, \dots., r_N) \qquad (1.1)$$

for N-electron atomic or molecular system. Where $\widehat{H}$ is Hamiltonian operator, Ψ is wave function of the system, and E is enegy. Hamiltonian operator is a sum of

the three terms given by

$$\widehat{H} = -\frac{1}{2}\sum_i^N \nabla_i^2 + \hat{V}_{ext} + \sum_{i<j}^N \frac{1}{|r_i - r_j|} \quad (1.\ 2)$$

where first term represents the kinetic energy,

$$\hat{T} = -\frac{1}{2}\sum_i^N \nabla_i^2 \quad (1.\ 3)$$

$\hat{V}_{ext}$ is the external potential operator. External potential is the interaction of the electrons,Z_α, with the atomic nuclei α, which is given by

$$\hat{V}_{ext} = -\sum_\alpha^{N_{at}} \frac{Z_\alpha}{|r_i - R_\alpha|} \quad (1.\ 4)$$

and the last term defines the electron-electron interaction V_{ee},

$$\hat{V}_{ee} = -\sum_{\alpha<\beta} \frac{Z_\alpha Z_\beta}{R_{\alpha\beta}}, \quad (1.\ 5)$$

(Parr and Yang, 1989). The exact solution of Schrödinger equation is only possible for small systems. Density functional theory (DFT) is an approach for the solution to Schrödinger equation.

1.5.2. Density Functional Theory

As mentioned before, the Density functional theory is currently the most effective method to compute the electronic structure of a system and based on two theorems of Hohenberg and Kohn and later developed by Kohn and Sham.

1.5.2.1. The Hohenberg Kohn Theorem

The main assumption of DFT, which shows that the ground state properties of a system are unique functionals of the ground state electron density, was proved by

Hohenberg and Kohn in 1964. The description of an interacting system of fermions via its density instead via its many-body wave function is the main idea of DFT.

Hohenberg and Kohn proposed the following theorem and proved in 1964,

1. Energy functional *E[n]* can be computed exactly from the ground-state electron density.
2. Second theorem states that the ground-state electron density can be calculated exactly using the variational method for minimization of the Hohenberg-Kohn functional (Ramanchandran, Deepa, & Namboori, 2008).

The total Hamiltonian in more compact form,

$$\hat{H} = \hat{T}_e + \hat{V}_{ext} + \hat{V}_{ee}. \quad (1.6)$$

As stated in the theorem, we can express the total ground state energy in terms of functionals of the ground state densities ρ_0,

$$E_0[\rho_0] = T_e[\rho_0] + V_{ext}[\rho_0] + V_{ee}[\rho_0] \quad (1.7)$$

From the second theorem, the ground-state electron density $\rho(r)$ determines the number of electrons *N* according to the conservation relation

$$N = \int \rho(r) dr \quad (1.8)$$

The minimization condition of energy functional is

$$\delta E[\rho(r)] = 0 \quad (1.9)$$

These were the first theoretical footings of DFT calculations and they are known as Hohenberg-Kohn theorems. Other framework, difficult many-body problem of interacting electrons is simplified to an easier problem of non-interacting electrons moving in an effective potential, is known as Kohn-Sham DFT (Kohn and Sham, 1965).

1.5.2.2. The Kohn and Sham Method

In the previous method, energy minimization is carried out according to the changing density. However, kinetic energy calculation from density is not accurate whereas calculation from wave function is easy and satisfactory. Therefore, Kohn and Sham combined the wave function and density approach in their method. In this theory, the effective potential includes the external potential and the Coulomb interactions between electrons are taken into account. Total energy functional can be rewritten as

$$E[\rho(r)] = T_0[\rho] + \int \left[\hat{V}_{ext}(r) + \hat{U}_{el}(r)\right]\rho(r)dr + E_{xc}[\rho] \quad (1.10)$$

where $T_0[\rho]$ denotes the kinetic energy of the electrons, but there is no electron-electron interaction, which is considered as noninteracting system. However, electron-nuclei interaction is taken into consideration with the Coulomb interaction between the electrons and V_{ext} accounts for the potential from the nuclei.

The last term $E_{xc}[\rho]$ is called as exchange-correlation energy**.** This term takes into account all other energy contributions that have not been considered by the previous terms.

However, the modelling of exchange and correlation interactions is very difficult within the Kohn-Sham method. In order to solve this problem, the local-density approximation (LDA) was introduce by Kohn and Sham along with their equations.

The LDA suggested that the exchange-correlation energy can be given by assuming for each infinitesimal element of density, the energy is that of a uniform electron gas of density. In LDA the exchange correlation functional is based on the exchange correlation energy $\varepsilon_{\mathrm{xc}}(\rho(r))$ of a homogeneous electron gas with the electron density $\rho(r)$

$$E_{xc}^{LDA}[\rho(r)] = \int \varepsilon_{\mathrm{xc}}(\rho(r))\rho(r)\,\mathrm{dr} \qquad (1.11)$$

in which the exchange correlation energy solely depends on the local electron density.

Despite a great success of LDA, this theory is not satisfying all the details of charge distribution, because charge density is highly non-uniform around atoms. This problem was solved by introducing the generalized-gradient approximation (GGA) (Perdew et al., 1992) where the spatial variation in the density is taken into account. The GGA significantly improved predicted binding and dissociation energies and here the functional depends on the local electron density as well as on its first derivative

$$E_{xc}^{GGA}[\rho(r)] = \int f(\rho(r), \nabla(r))\mathrm{dr} \qquad (1.12)$$

Exchange correlation of the system is correlated with both density and derivatives of density. Thus, more accurate results are obtained with GGA method (Parr and Yang, 1989; Jensen, 2007; Ramanchandran, Deepa, & Namboori, 2008; van Santen and Sautet, 2008).

1.5.3. Pseudopotentials

The pseudopotential is a fictional potential that is constructed from the nucleus and the core electrons. The electronic wavefunctions would be represented accurately numerous plane waves. A combination of pseudopotentials and fast-Fourier transforms (FFT) are used to overcome this problem. FFT enables the

transformation of the wavefunctions and charge density between real and reciprocal space. Thus, the calculation scale of the problem take place in two different spaces, and therefore they are carried out in the ‘cheaper’ space.

1.6. Objective of the Study

It is well known that rare earth dopant enhances the thermal stability and OSC of CZO catalyst as stated in the literature. However, in the view of the literature findings, the reaction mechanisms and the electronic effect of these improvement are unclear. Additionally, there has been little study on the investigation of the effect of La doping on catalytic activity. Furthermore, there is no theoretical study in the open literature on La doped CZO catalyst. To that end, the main objective of this theoretical study is to investigate CO oxidation in La and Pd+La doped TWC system by using DFT methods of computational chemistry. For this purpose, Vienna Ab initio simulation Package is used for the computer application of DFT methods. La and Pd+La doped ceria-zirconia catalyst surfaces are prepared. Then, these surfaces are investigated for CO oxidation reactions. Relative energy profiles and activation barriers of CO adsorption and desorption reactions steps on these surfaces are obtained and compared. Promotional effect of La doping is investigated. Thus, with the help of the results of this study, novel TWC configurations may be determined for catalytic performance before experimental research.

CHAPTER 2

LITERATURE REVIEW

Since the early 1990s, ceria-zirconia mixed oxides has been used in the TWCs instead of pure ceria due to pure ceria's poor thermal instability. The insertion of zirconia (ZrO_2) in ceria (CeO_2 enhances the thermal stability, surface area and oxygen storage capacity of the catalyst (Kaspar et al., 1999). Ceria-zirconia system also shows better redox properties than that of pure zirconia because of higher defect sites leading to increase in oxygen vacancy generation (Damyanova et al., 2007).

Different compositions of Ceria-Zirconia (CeO_2-ZrO_2) automotive catalysts combined with other metal atom substitutions and promoters have been investigated by many researchers in terms of their catalytic activity and stability.

2.1. Ceria-Zirconia in TWC

The CeO_2-ZrO_2 solid solutions impregnated on γ- Al_2O_3 is investigated by by Di Monte et al. (2000). They proved the positive effect of impregnation of γ- Al_2O_3 with cerium-zirconium on the oxygen storage capacity even after calcination.

Kaspar et al. (2002) synthesized different compositions of $Ce_xZr_{1-x}O_2$ using citrate complexation method to investigate the effect of ZrO_2 content on textural and structural properties of CZO solid solutions. They suggested that cerium rich compositions can be good candidates for catalytic applications at low to medium temperature.

NO reduction by CO over Pd-Al_2O_3 and Pd-$Ce_{0.6}Zr_{0.4}O_2/Al_2O_3$ catalyst was studied by Di Monte et al. (2002) to investigate the effects of $Ce_{0.6}Zr_{0.4}O_2$ addition to Pd-Al_2O_3 catalyst. They pointed out that the $Ce_{0.6}Zr_{0.4}O_2$ addition strongly affects the surface Pd species under reaction conditions. The activity of catalyst is improved below 500 K; catalytic activity is not affected by support above 500 K; and oxidized Pd species are stabilized at catalytic surface. In the case of zirconia addition, due to the direct interaction of Pd species with oxygen species of the support, CO removal rate is promoted by these oxygen species. The removal of surface adsorbed CO/NO species is observed more easily compared to zirconia absent catalyst.

Gayen et al. (2006) investigated the activity of Rh-Pt catalysts for TWC. It is observed that main synergistic effect is caused by Rh^{3+} ion reduction at lower temperature in the presence of Pt^{2+} ions. Bimetallic catalysts show better performance in the oxidation of CO, and NO and C_2H_4 reduction improved compared to the monometallic catalysts.

2.2. The Effect of Metal Atom Substitution

The effect of metal atom substitution to CeO_2-ZrO_2 catalyst has been investigated by many researchers. Early studies on the effect of rare earth dopants were on Pd/Al_2O_3 catalyst.

XPS and TPR studies were carried out by Muraki et al. (2001) to investigate the catalytic effects of La_2O_3 on Pd/Al_2O_3 catalyst for the NO reduction. They observed that NO reduction enhances with the addition of lanthana. As a result of XPS and TPR studies, hydrocarbon chemisorption and therefore catalyst poisoning are suppressed by the addition of lanthana.

The previous work of Muraki et al. (1986) also indicates that the reduction of NO is inhibited by hydrocarbons on Pd-La_2O_3/Al_2O_3 catalyst. In the presence of La_2O_3, NO reduction was better compared to Pd-only catalyst. This may occur due to the weakening adsorption strength of HCs with the Pd-La cooperation. NO reduction by H_2 is observed as highly selective and fast.

Yao et al. (2011) also explained the positive catalytic effect of the addition of La_2O_3 to the Pd-based catalyst C_3H_8 conversion after aging. They found that Pd dispersion and reducibility are higher than that of the La_2O_3 absent catalyst.

Another investigation on the effect of La_2O_3 addition to the catalytic activity of Pd-Al_2O_3 catalyst was conducted by Kim et al. (2000). They prepared Pd-La_2O_3/Al_2O_3 catalyst by co-impregnation, and Pd/La_2O_3/Al_2O_3 catalyst by sequential impregnation, methods. The co-impregnated catalyst had better light-off performance than that of the catalyst prepared by the sequential impregnation. Although Pd-La_2O_3/Al_2O_3 lost its surface area after thermal aging, it conserved its superior activity. As a promoter La_2O_3 improves the thermal stability of Pd-La_2O_3/Al_2O_3 catalyst through the close interaction with Pd during thermal aging while suppresses the relation between PdO and alumina. However, in the case of Pd/La_2O_3/Al_2O_3 catalyst, lanthana interacts with the alumina during the thermal aging and stabilizes the support.

Skoglundh et al. (1996) compared Pd alone and La doped Pd-alumina catalyst in terms of light-off performance and redox properties. They observed that the addition of La widen the interval compared to Pd alone catalyst under reducing conditions. Additionally, NO conversion is improved by the addition of lanthanum. They explained that better NO conversion is as a result of the formation of Pd-La oxide or alloy which favors the reduction reaction of NO by CO instead of the reaction between CO and O_2.

NO chemisorption on the Pd (100) surface with ultra-thin over layers of La_2O_3 and Al_2O_3 was studied by Logan and Graham (1989). NO was partial dissociation of NO was observed on La_2O_3 over layers whereas it is nondissociative on Al_2O_3 over layers at 300 K, which suggests that La contributes to dissociative adsorption of NO on Pd (100) surface.

With the replacement of alumina catalyst with ceria-zirconia catalyst, the effect of rare earth dopants on CZO have been started to be investigated in detail. Additionally, it is known that the performance of Pd in CZO catalyst can be improved by introduction of a promoter (Wang et al., 2015). The effect of the introduction of La_2O_3 to Pd based catalyst on the catalytic activity has also been studied various researches by experimentally.

Vidmar et al. (1997) studied the OSC of $Ce_{0.6}Zr_{0.4}O_2$ catalyst doped with three valent cations such as La, Nd, and Y. OSC of the doped system at low temperature is improved by 30% compared to undoped catalyst. They also observed that all dopants stabilize CeO_2 with respect to high temperature calcination. Surface La content increases with the calcination with respect to bulk La concentration.

A series of $Ce_{0.2}Zr_{0.8}O_2$ catalyst containing different amount of La have been prepared by Wang et al. (2010). In their experimental research, the effect of La content in CZO on the catalytic activity was investigated. They observed that La content contributes to conversion of all target compounds on the aged catalysts and fresh samples are successful on NO reduction.

Another important study was also carried out by Wang et al. (2011). In this study, a series of $Ce_{0.2}Zr_{0.8}O_2$ (CZO) doped with rare earth metals of La, Nd, Pr, Sm, and Y were prepared and their characterization were carried out. The metal atom doping effect on OSC and thermal stability of the solid solution were investigated. The catalytic performance over a wide air to fuel operating window were also examined. The major findings of this study are summarized in Figure 2.1.

It is reported that the presence of La, Nd and Pr improves the thermal stability of CZO catalyst. It also improves the reducibility.

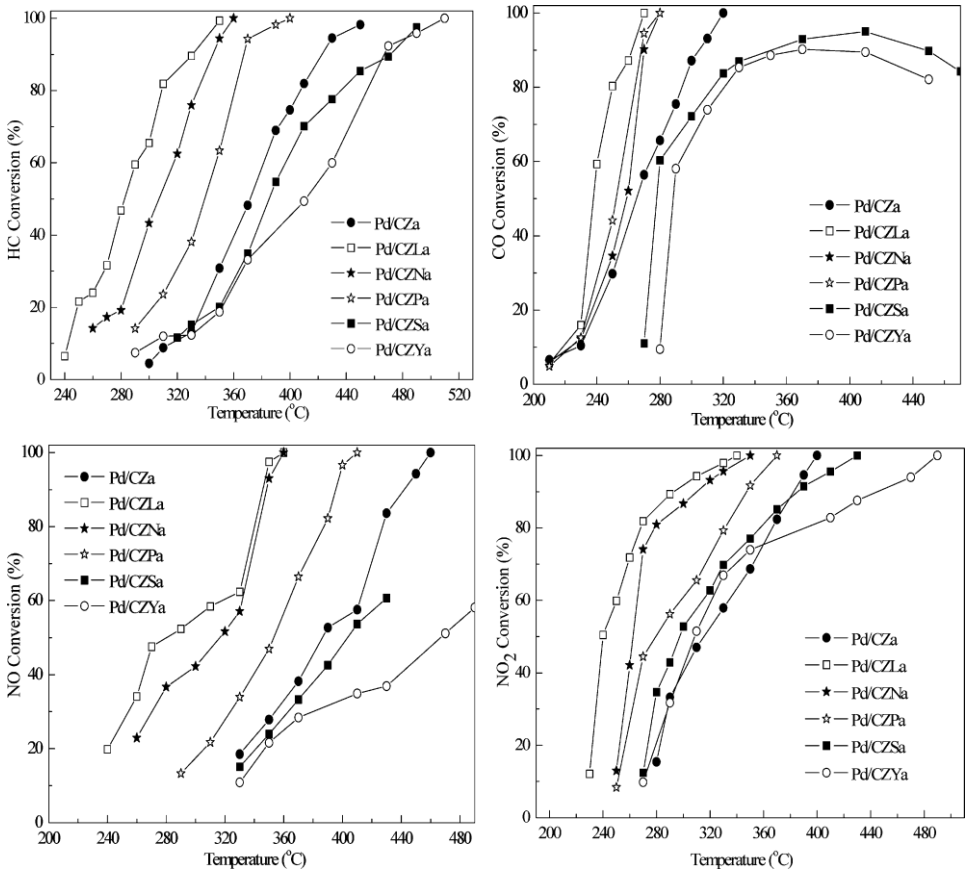

Figure 2.1 Catalytic performance of $Ce_{0.2}Zr_{0.8}O_2$ modified of rare earths.

Due to increased metal support interaction, relatively higher three-way catalytic activity is observed for all of the target pollutants.

In a later study of the research same group, Wang et al. (2011), the effect of rare earth (La, Nd, Pr, Sm, and Y) addition to $C_{0.2}Zr_{0.8}O_2$ and Pd based $C_{0.2}Zr_{0.8}O_2$ catalyst was investigated. They observed that the stability, reducibility and metal-support interaction of CZO catalyst increase in the presence of rare earth metal leading to higher catalytic performance for all target pollutants. The air to fuel ratio window increases with increasing dynamic oxygen storage capacity.

Zhao et al. (2013) also studied $C_{0.67}Zr_{0.33}O_{2-x}$ catalyst to investigate the effect of catalytic activity of rare earth modification. For this reason, Ce-Zr-M (M= La, Pr, Nd, Sm, and Y) ternary mixed oxides were prepared and used as support. Since ceria is rich in the support, the cubic structure is featured in the structure as observed from XRD results. The incorporation of rare earth metal into ceria-zirconia improves the oxygen storage capacity and the interaction between PdO species and support. The main reason of this increase is due to the relatively higher concentration of Ce^{3+} species on the catalyst surface with the addition of rare earth metal. Superior activity for NOx and HC conversion is observed after aging treatment, especially for the catalyst containing Pr or Nd.

Guo et al. (2007) investigated the effect of La_2O_3 on the performance of Pd/ceria-zirconia catalyst. In this experimental study, $Ce_xZr_{1-x}O_2$ nanoparticles (x = 0.75, 0.62) were prepared. The activity of Pd-only three-way catalyst was tested in the fixed-bed reactor. The composition of simulated exhaust gas is 3% CO, 5000 ppm C_3H_8, 5000 ppm NO, 10% CO_2, O_2 and N_2 gases. They found that the light-off performance of the catalyst is decreased by the addition of La_2O_3. However, the oscillation of the conversion of NO and HCs are suppressed. After the aging of catalyst, the operating window turned to lean burn.

These experimental studies address that the interaction between lanthanum and the support material enhances the activity of TWC catalyst.

2.3. Density Functional Theory Studies

There has recently been great interest in theoretical studies with the increased computer capacity and development in DFT techniques over last decades. Recent DFT studies on the development of CZO catalyst with regard to CO oxidation are summarized below.

Fe-modified CeO_2 (111) surface is studied to investigate the mechanisms for the CO oxidation by Chen and Chang (2011). They used periodic density functional

theory corrected for the on-site Coulomb interaction by a Hubbard term (DFT+U). They observed that Fe is stable both as an adsorbed atom on the surface and as a dopant in the surface region. Oxygen vacancy formation is facilitated by dopant Fe atoms, while Fe adatoms might suppress oxygen vacancy formation. Physisorbed CO_2 and chemisorbed CO (carbonate) species are observed on the Fe doped CeO_2 (111) surface, whereas, on the clean surface, only physisorbed CO is observed.

Another DFT+U study was performed by Wang et. al (2009) to investigate the effect of Zr doping on the oxygen storage properties of several $Ce_{1-x}Zr_xO_2$ surfaces (x=0.75, 0.50, 0.25). They found that bond energies of Zr-O species increase with the increasing amount of Zr. However, relaxation energies follow a parabolic profile with a minimum value for for the catalyst of x=0.5. Vacancy formation by decomposing it into two terms: the bond energy and relaxation energy. They concluded that the relaxation energy is more dominant parameter than bond energy; therefore, equimolar Ce and Zr concentration in CZO catalyst exhibit the highest oxygen storage capacity.

Nolan et al. (2005b) studied the lattice parameter of bulk ceria using DFT methods implemented on VASP. The computed lattice parameter is 5.470 Å, which is consistent with the experimental value of 5.411 Å. They also investigated the relative stability and oxygen vacancy formation energy of (111), (110) and (100) surfaces (Nolan et. al, 2005a). The surface stability is in the order of (111)> (110) > (100), whereas the (110) ceria surface has the lowest vacancy formation energy and therefore the most reactive surface.

Introduction of noble metals such as Pd, Pt and Rh to ceria catalyst is also studied by several researches with DFT methods.

Pd doped ceria (111) surface was investigated by Yang et al. (2007) by DFT method implemented in VASP. PAW method and GGA approximation is used. Pd

atom is adsorbed on different surface sites. It is observed that Ce-O bridge position in these sites is most favorable.

Gerceker and Önal (2013) investigated CeO_2 and $Ce_{0.75}Zr_{0.25}O_2$ surfaces with the modification by Pd_4 and Rh_4 metal clusters adsorption and Pd and Rh substitution in terms of CO oxidation mechanisms. DFT are used to model the surfaces and reaction mechanisms with the help of computer program VASP based on PAW method and GGA approximation. Oxygen vacancy formation energy was calculated as 43.7 kcal/mol for Pd substituted CZO surface. On this surface the activation barrier is reported 45 kcal/mol between the steps of first CO adsorption and desorption of CO_2.

CO oxidation on Mn doped ceria (111) surface was studied by Hsu et al. (2012). They compared the activation barrier of CO2 desorption for Mn adatom and Mn atom substituted surfaces. On the Mn atom substituted surface, no CO_2 desorbs creating oxygen vacancy with no activation barrier, whereas Mn adatom Mn adatoms restricts the vacancy formation energy and the activation barrier is calculated as 0.84 eV.

Civan (2014) studied the effect of CO oxidation mechanisms on Mn doped $Ce_{0.75}Zr_{0.25}O_2$ (110) surfaces. For this purpose, Mn, Mn-Pd, and Mn-Rh doped surfaces was prepared. According to relative energy profile calculations, Mn-Pd doped surface is found to be energetically most favored. The activation barrier of CO_2 desorption step is overcome with the incorporation of Mn and Pd on this surface.

Yeriskin and Nolan (2009) investigated the effect of lanthanum doping on CO adsorption at La-doped Ceria (111) and (110) surfaces using DFT+U method. It is observed that La^{3+}-O^- defect state forms with doping with La^{3+} at both (111) and (110) surfaces. At the undoped (111) surface, CO only weakly physisorbs, while strong adsorption of CO is observed at doped surface resulted in direct CO_2 formation.

Formation of monodentate or bidentate carbonate species depends on the oxygen vacancies on doped (110) surfaces. At (110) and (111) surfaces, CO interaction with the surface is improved over the corresponding undoped surfaces. It is observed that the theoretical findings are consistent with experimental results, and also the results obtained from other dopants in ceria.

In another study of the same authors (2010), they point out that oxygen vacancy formation energy is reduced with the substitution of lanthanum. Energy requirement for the formation of an oxygen vacancy in La-doped structure is at least 0.90 eV on (111) surface and 0.64 eV on (110) surface. It is seen that these values are small enough and vacancy formation will be enhanced compared to the undoped surfaces. As a result, they concluded that La-doping of ceria surfaces shows enhanced reactivity over the undoped surfaces.

Experimental and theoretical studies suggest that metal atom substitution enhances the catalytic activity of CZO catalyst. To that end, in this study, the effect of La doping on the catalytic activity of ceria-zirconia catalyst has been investigated. Comparison of the activities of La and Pd doped CZO surfaces in terms of CO oxidation has been carried out.

CHAPTER 3

COMPUTATIONAL METHODOLGY

In this research study, Density Functional Theory methods are implemented in Vienna Ab initio Simulation Package (VASP). Starting with the bulk structure optimization of support material, two different surface planes are cleaved from the bulk with required depth and these surfaces are also optimized. Then, metal atom substitutions on these surfaces are carried out. The catalytic performances of the surfaces in terms of CO oxidation are investigated on these surfaces. For this purpose, gas phase reactants are optimized and proposed reaction mechanism steps are modelled. CI-NEB method is used to predict activation barriers of the reaction steps.

3.1. Vienna Ab initio Simulation Package (VASP)

There are quite a number of computational software packages that use methods of theoretical chemistry to calculate structures and properties of molecules and solids. In this study, quantum mechanical calculations are implemented in Vienna ab Initio Simulation Package (VASP) code, (Kresse and Fürthmüler 1996; Kresse and Hafner 1993), based on DFT formalism.

The computational procedure of the VASP code includes an iterative solution of the Kohn–Sham equations based on residuum-minimization and optimized charge-density mixing routines. The total energy is optimized with respect to the positions of the atoms within unit cell or supercell. The electron exchange and correlation are treated within the generalized gradient approximation (GGA), (Perdew, & Chevary, 1992), using projector augmented approximations (PAW)

method (Blöch 1994; Kresse, & Joubert, 1999). VASP code employs DFT method in a periodic manner. Specifically, the code gives more accurate results for solid systems, such as metal oxides, that have periodic boundary conditions.

To perform VASP code, several input information of the system are required. These are initial positions of the atoms, pseudopotentials, specified k-points mesh values and keywords for convergence.

Depending on the given input information, the outputs of VASP are several: energy and force, volume, density of states, charges, optimized geometry of the structure, vibrational frequency, and so on. The program performs the minimum energy optimization. The key parameters determining the convergence of VASP are the number of basis functions (plane wave cutoff) and the number of k- points (k-spacing).

3.2. Simulation Procedure Using VASP

In this study, DFT simulation of CO oxidation on $Ce_{0.75}Zr_{0.25}O_2$ (110) surfaces are carried out in VASP code using the generalized gradient approximation (GGA) and projector augmented-wave (PAW) method.

In the computations, Mankhorst-Pack k-point mesh is selected (19x19x19) for bulk optimizations, (4x4x1) for surface optimizations, and (1x1x1) for gas phase molecules optimizations (Monkhorst and Pack, 1976) in order to determine the integration points. In structural optimizations, convergence criterion is determined as 0.015eV/Å for the net force acting on each atom. Energy cut-off is set to 500eV for the calculations.

First, the optimization of bulk CeO_2 is performed using lattice parameter reported in the literature. After obtaining the optimized lattice parameters, CeO_2 bulk is created and cleaved for CeO_2 (110) surface with the depth of 6 atomic layers as a (3x2) supercell.15 Å vacuum space is added on top of the surface to avoid any

interaction with the periodically continuing upper layers. The bottom layer is kept fixed to describe the bulk structure while others are fully relaxed.

$Ce_{0.75}Zr_{0.25}O_2$ stoichiometry is obtained by replacing one of the Ce atoms in each layer with a Zr atom. La and Pd atom substitutions are carried out in the same way; one or two Ce atoms on the top layer were exchanged with La and Pd atoms and then further optimized. Similarly, at the bottom layer, atoms are kept fixed to represent of a bulk structure of catalyst surface while the atoms in remaining layers were fully relaxed.

After the optimization of surface models, CO adsorption and desorption were computed on these optimized surfaces. Gas phase CO reactant and CO_2 product molecules are optimized in a 10Å x 10Å x 10Å vacuum cell. Relative energy of each reaction step is calculated with the following equation

$$E_{rel}=E_{system}-(E_{surface}+\Sigma E_{reactants}) \quad (3.1)$$

where E_{system} is the energy of the overall molecular system, $E_{surface}$ is the optimized surface energy and $\Sigma E_{reactants}$ are energies of the optimized gas phase reactants.

Activaiton barrier calculation for a reaction, Climbing Image Nudged Elastic Band method (CI-NEB) is used (Henkelman et al., 2000). This method finds the saddle point and minimum energy paths between known initial and final steps of the reaction. After creating a specified number of images with equal distances from each other, these intermediate images are optimized. The structure with the highest energy is considered as the transition state structure. Consequently, the approximate activation barrier energy of the reaction is obtained by using the energy of transition structure. The transition state structure are optimized again to verify that it is a first order saddle point. Sample input scripts used in the computations are given in Appendix A.

CHAPTER 4

THEORETICAL MODELING OF THREE WAY CATALYST

4.1. Bulk Structure Optimization of Cerium-Zirconium Oxide

Cerium oxide is a rare earth oxide having fluorite type structure with space group Fm3m. It contains cubic closed-packed metal atoms with oxygen atoms placed in all tetrahedral holes (Trovarelli, 1996). Experimental value of lattice parameter of CeO_2 crystal is 5.411 Å (Trovarelli, 1996). The oxygen - oxygen distance is 2.705 Å, which is half the lattice parameter. Ce-Ce and Ce-O bond lengths are 3.86 and 2.36 Å, respectively.

Modelling of TWC starts with the optimization of cerium oxide (CeO_2) unit cell. Lattice parameter of CeO_2 is computed as 5.464 Å which is consistent with the experimental value.

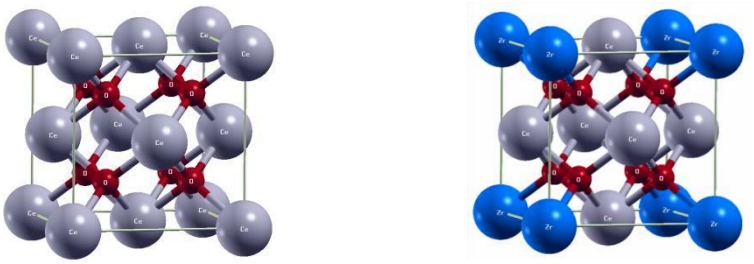

(a) **(b)**

Figure 4.1 Optimized bulk (a) CeO_2 unit cell, (b) $Ce_{0.75}Zr_{0.25}O_2$ unit cell.

Cerium-zirconium oxide is obtained in the stoichiometric ratio $Ce_{0.75}Zr_{0.25}O_2$ (CZO) by replacing one out of four Ce atoms in the unit cell of CeO_2 with one zirconium atom. $Ce_{0.75}Zr_{0.25}O_2$ unit cell lattice parameter is computed as 5.379 Å, which is also consistent with the experimental value of 5.39 Å (Yang et al., 2009). The decrease of the CZO unit cell size is due to the surface strain caused by substitution of zirconium substitution (Wang et al., 2009). CeO_2 and $Ce_{0.75}Zr_{0.25}O_2$ unit cells are shown in Figure 4.1.

In models, Ce atom is represented by gray ball, Zr blue, Pd pink, La orange, carbon yellow, and oxygen red.

4.2. Surface Slab Optimizations

The surface energy quantifies the energy loss for disruption of chemical bonds that occur when a crystal is cleaved and a surface is created. It is calculated per unit area of a surface as the difference between the energy of the system terminated by the surfaces (slab) and the system of the same number of unit cells within the bulk.

Slabs used in ab initio calculations have finite thickness, which has to be chosen large enough, so that the surface energy reaches its convergence level.

As the results of calculation on different surfaces, the (111) surface is found as energetically the most stable surface followed by (110) and (310) surfaces, and accordingly less reactive. In other words, (110) and (310) surfaces make more reactive catalyst (Alessandro Trovarelli, Paolo Fornasiero). Therefore, in this study, (110) surface is used in the computations cleaving from bulk Ceria with 6 atomic layers. Then, the (110) ceria surface is doped with zirconia. The optimized surfaces are sown in Figure 4.2.

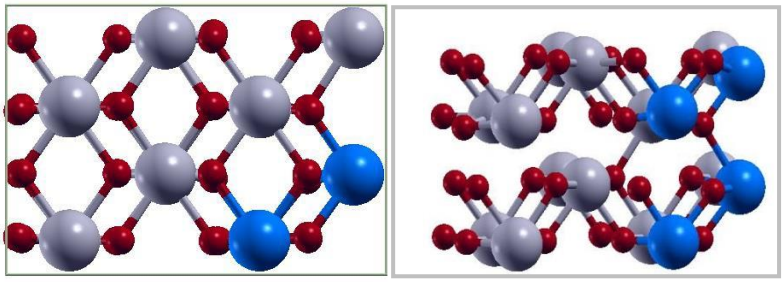

(a) **(b)**

Figure 4.2 (a) Top and (b) side view of $Ce_{0.75}Zr_{0.25}O_2$

4.3. Metal Atom Substitutions to $Ce_{0.75}Zr_{0.25}O_2$ (110) Surfaces

Single metal atom of La and both Pd and La are substituted on $Ce_{0.75}Zr_{0.25}O_2$ (110) surface to investigate the catalytic activity of rare earth metal. The surfaces are obtained by replacing cerium atom at the top layer with dopant atom.

After the metal introduction to the catalyst surface, energy change of each surface due to metal atom substitution is calculated using the following equation

$$\Delta E_{substitution} = E_{M-surf} + E_{Ce} - (E_{surf} + E_M) \quad (4.1)$$

where, E_{M-surf} is the energy of the surface doped with a metal atom, E_{surf} the energy of undoped surface, E_{Ce} and E_M are the energies of single cerium atom and the dopant metal atom, respectively. The single atoms are also optimized in a vacuum cell.

4.3.1. Pd Substitution on $Ce_{0.75}Zr_{0.25}O_2$ (110) Surface

Pd doped CZO surface is prepared by positioning Pd and Zr atoms aligned with each other. To obtain this configuration, one cerium atom at the top layer with a Pd atom is replaced with one Ce atom. Figure 4.3 depicts top and side views of Pd-CZO (110) surface.

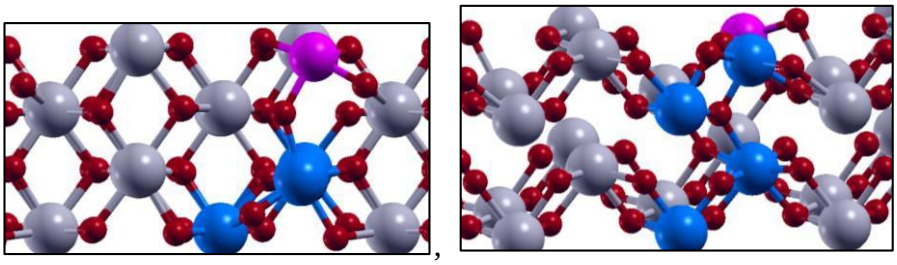

Figure 4.3 Pd doped CZO surface, top and side views, respectively.

4.3.2. La Substitution on $Ce_{0.75}Zr_{0.25}O_2$ (110) Surface:

Lanthanum doped surface is prepared in the same way of Pd doped CZO surface. La and Zr are aligned with each other on the surface. In this case, one cerium atom is replaced with a La atom at the top layer. Top and side view of optimized La-CZO (110) surface is given in Figure 4.4.

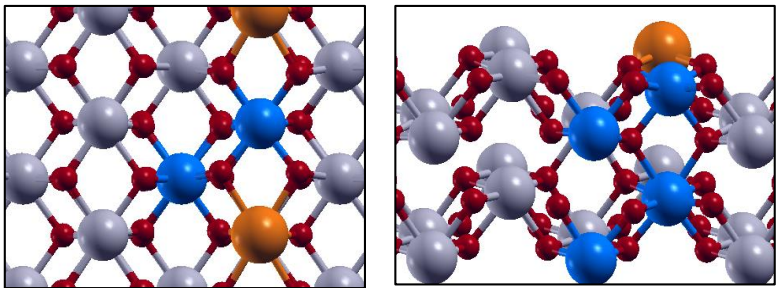

Figure 4.4 La doped CZO surface top and side views, respectively.

4.3.3. Pd+La Substitution on $Ce_{0.75}Zr_{0.25}O_2$ (110) Surface:

In this case, bimetallic doped catalyst surface is prepared. For this reason, CZO (110) surface doped with both Pd and La atom by replacing with two cerium atoms on the upmost surface. As shown in Figure 4.5, Pd, Zr and La atoms are diagonally positioned over the surface.

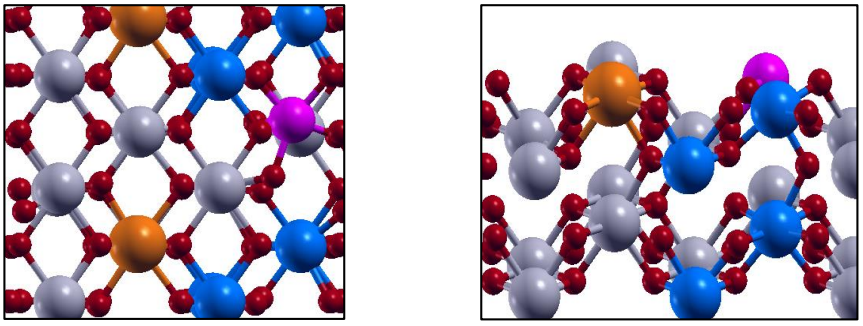

Figure 4.5 Both Pd and La doped CZO surface top and side views, respectively.

In the doping process, to remove and substitute another atom requires energy. To calculate the energy changes of metal substituted surfaces with respect to bare CZO surface, Eq. 4.1 is used and results are listed in Table 4.1.

Table 4.1 Energy changes of surfaces due to atomic substitution

Surface	Energy change (kcal/mol)
Pd-CZO (Gerceker, 2013)	295.514
La-CZO	63.14701
Pd-La-CZO	361.1463

Experimental studies revealed that La introduction into CZO lattice is facile (Wang et al., 2010), which is verified by current study with DFT computations. The minimum energy changes is observed in the case of La atom substitution on CZO surface, which is 63.147 kcal/mol. Since La has a similar atomic radius to

that of Ce atom, its substitution does not require high energy compared to Pd substitution (295.514 kcal/mol). However, bi-metallic substitution requires more energy and may be the most difficult one. As a result, La substitution is energetically more favorable than those of Pd and bimetallic substitution.

4.4. Optimization of Gas Phase Molecules

In CO oxidation reaction, CO is reactant and CO_2 is product. Their energies are required in the calculation of relative energies. The gas phase CO and CO_2 molecules are optimized in a 20Å×20Å×20Å vacuum cell and gas phase formation energies are calculated. Optimize CO and CO_2 molecules are given in Figure 4.6.

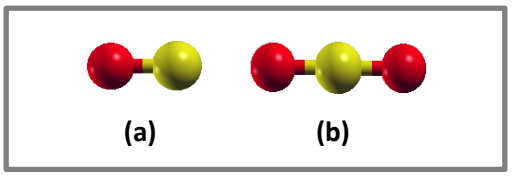

Figure 4.6 Optimized (a) CO, and (b) CO_2 molecule in the gas phase.

C-O bond length is calculated as 1.14Å and 1.18Å in CO and CO_2 molecules, respectively. Calculated gas phase energies are -340.34 kcal/mol (-14.79 eV) and -528.7 kcal/mol (-22.99 eV) for CO and CO_2 molecules, respectively.

CHAPTER 5

RESULTS AND DISCUSSION

In this phase of the study, CO oxidation reaction steps and energetics on the optimized CZO surface models are investigated. The results obtained in this part are compared with the previously reported findings of Pd substituted $Ce_{0.75}Zr_{0.25}O_2$ (110) (Gerçeker and Onal, 2013) and Mn doped $Ce_{0.75}Zr_{0.25}O_2$ (110) (Civan, 2014) surfaces in terms of CO oxidation.

5.1. CO Oxidation on La-$Ce_{0.75}Zr_{0.25}O_2$ (110) Surface:

To investigate the catalytic activity of atomic lanthanum doped $Ce_{0.75}Zr_{0.25}O_2$ (110) surface in terms of CO conversion, one cerium atom on the CZO surface is replaced by a palladium atom. On the La-CZO surface, dopant lanthanum atom and zirconium atom of the top layer are aligned.

Energies of CO adsorption and CO_2 desorption steps are calculated relative to bare La-CZO surface energy. Reaction steps and relative energies of CO oxidation mechanism on La-$Ce_{0.75}Zr_{0.25}O_2$ surface are given in Table 5.1.

Table 5.1 CO oxidation on La-$Ce_{0.75}Zr_{0.25}O_2$ surface

Reaction Step	Relative Energy (kcal/mol)
R1: $CO_{(g)} \rightarrow CO_{(ads)}$	-86.967
R2: $CO_{(ads)} + O_{lat} \rightarrow CO_{2(g)}$	53.363

The first step of CO oxidation reaction begins with the approaching of a gas phase CO molecule to the surface. CO strongly interacts with the surface and it is adsorbed as carbonatelike species shown in Figure 5.1. It is bound on Ce-O bridge position next to the palladium atom creating carbonate species on the surface. To form this adsorption configuration, carbon atom pulls two oxygen atoms out of the CZO surface. The C-O bond lengths of the adsorbed CO molecule were found to be 1.317 Å on the ceria side and 1.331 Å on La side. Optimized gas phase CO approaching to the surface and adsorbed CO on the surface are shown in Figure 5.1. The adsorption step is exothermic with the approximate energy of -86 kcal/mol.

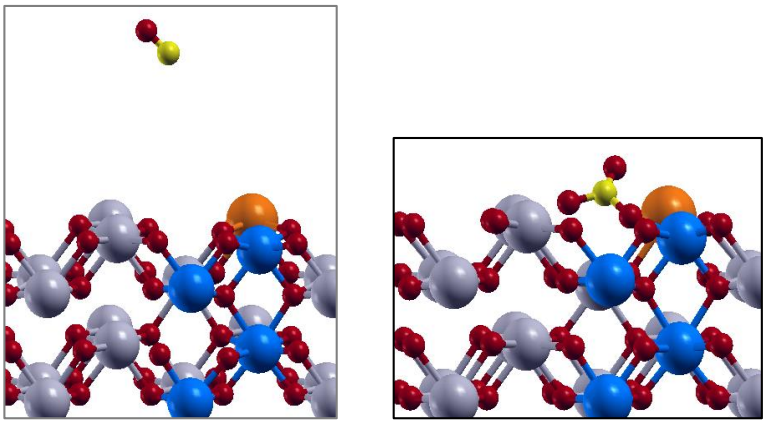

Figure 5.1 (a) CO molecule in gas phase, (b) CO adsorption on La-$Ce_{0.75}Zr_{0.25}O_2$ Surface

CO_2 is then released to gas phase with the labelled step R2 creating oxygen vacancy on the surface. Figure 5.2 shows CO_2 desorption step and the surface oxygen vacancy.

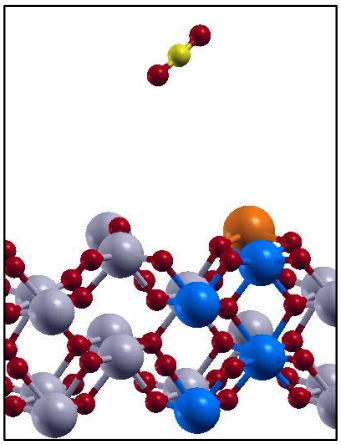

Figure 5.2 Desorbed CO_2 molecule in gas phase on La-$Ce_{0.75}Zr_{0.25}O_2$ Surface

Relative energy profile of first CO Oxidation on La-CZO surface is given in Figure 5.3. Approximately 30 kcal/mol energy required for the CO_2 desorption step. However, there is no activation barrier is observed at the CO_2 desorption step according to CI-NEB analysis. Oxygen vacancy formation energy is calculated as 34.49 kcal/mol.

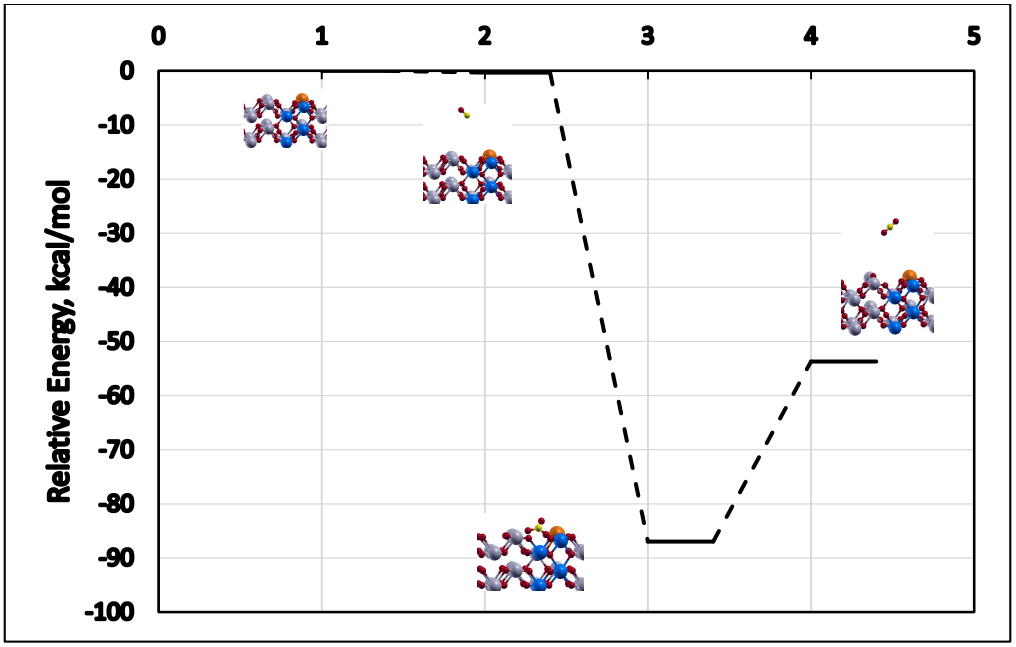

Figure 5.3 Relative energy profile of CO Oxidation on La- $Ce_{0.75}Zr_{0.25}O_2$ Surface

As reported in the study of Gerceker and Önal (2013), an activation barrier of 45 kcal/mole for CO_2 desorption step on the Pd- $Ce_{0.75}Zr_{0.25}O_2$ surface is calculated. As a result of current study, by means of doping CZO surface with La, activation barrier for CO_2 desorption has been overcome.

5.2. CO Oxidation on Pd+La-$Ce_{0.75}Zr_{0.25}O_2$ (110) Surface:

To investigate the contribution of La doping to the catalytic activity of Pd-CZO catalyst in terms of CO oxidation, Pd+La-$Ce_{0.75}Zr_{0.25}O_2$ (110) surface is prepared. One cerium atom is replaced by a palladium atom, and the other cerium atom diagonal to the palladium atom is replaced by one lanthanum atom on the CZO surface. Energies of each step are calculated relative to Pd+La-$Ce_{0.75}Zr_{0.25}O_2$ surface energy. CO adsorption and CO_2 desorption reaction steps and corresponding relative energies on Pd+La-CZO surface are given in Table 5.2.

Table 5.2 First step of CO oxidation on Pd+La- $Ce_{0.75}Zr_{0.25}O_2$ Surface

Reaction Step	Relative Energy (kcal/mol)
R1: $CO_{(g)} \rightarrow CO_{(ads)}$	-125.036
R2: $CO_{(ads)} + O_{lat} \rightarrow CO_{2(g)}$	-96.687

CO oxidation on the surface begins with approaching gas phase CO molecule to the surface. CO molecule is absorbed exothermically at the Ce-O bridge site next to the palladium atom as shown in Figure 5.4, this step is labelled as R1 and it is highly exothermic with the energy of -125 kcal/mol. Length of carbon-oxygen bond is 1.36 Å in both sides. Optimized geometries of CO molecule approaching the surface, and adsorbed molecule are shown in Figure 5.4.

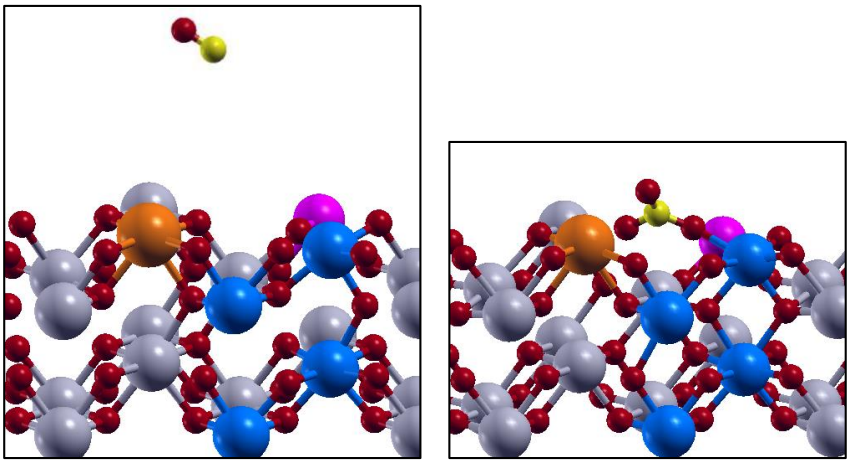

Figure 5.4 (a) Gas phase CO and (b) CO adsorption on Pd+La-$Ce_{0.75}Zr_{0.25}O_2$ surface.

Then, CO molecule desorbs from the surface forming CO_2 molecule to the gas phase. At this step, one of the surface oxygen atoms is pulled off by C atom and surface oxygen vacancy is created. CO_2 is then released to gas phase creating an oxygen vacancy. This step requires approximately 30 kcal/mol energy. The vacancy formation energy is computed as exothermic with a negative value of -4.30 kcal/mole at this surface. Desorption of CO_2 from the surface and oxygen vacant surface are shown in Figure 5.5.

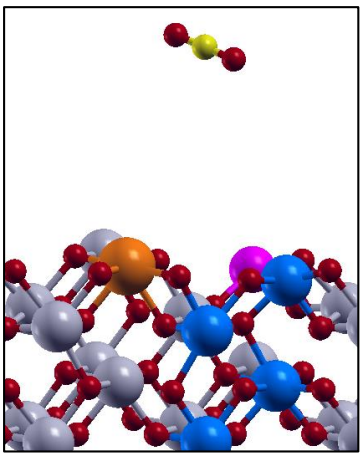

Figure 5.5 Desorption of CO_2 molecule from Pd+La-$Ce_{0.75}Zr_{0.25}O_2$ surface.

Relative energy profile of CO adsorption on Pd+La-CZO surface is shown in Figure 5.6. At the CO_2 desorption step, CI-NEB analysis is carried out for the activation barrier analysis. At this step, the high activation barrier is observed. According to experimental study of Guo et al. (2007), the lanthanum doping decreases the performance of Pd-CZO catalyst. This experimental phenomenon is verified by theoretically in this study. However, as reported in the same study, NO reduction enhances in the case of La doping. Therefore, further theoretical study is needed to explain the electronic effect of La contribution to NO reduction.

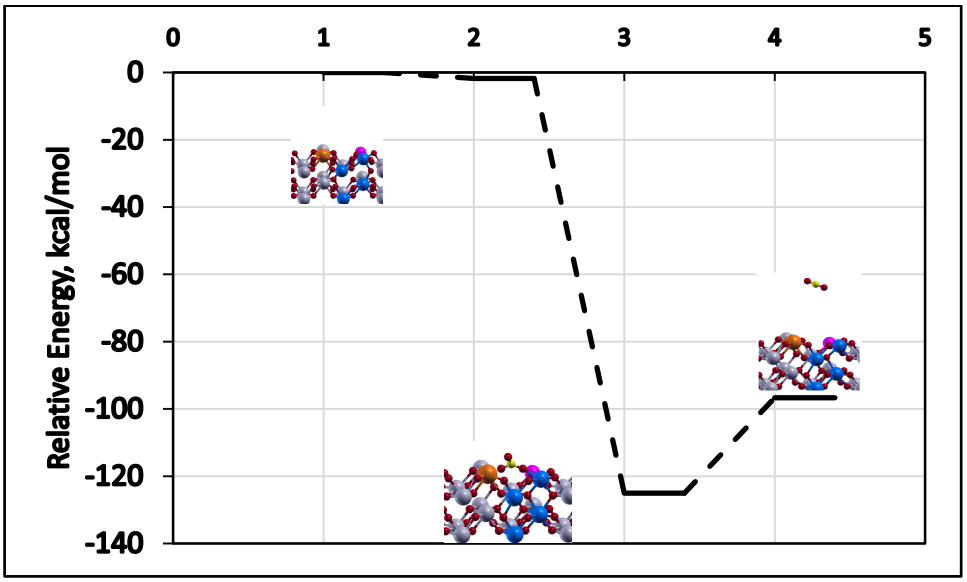

Figure 5.6 Relative energy profile of CO adsorption on Pd+La-CZO surface.

The relative energy profiles of both La-CZO and Pd+La-CZO surfaces are given in Figure 5.7. As shown in this figure, CO adsorption step is more exothermic on Pd+La-CZO surface compared to Pd absent surface while desorption requires almost same amount of energy.

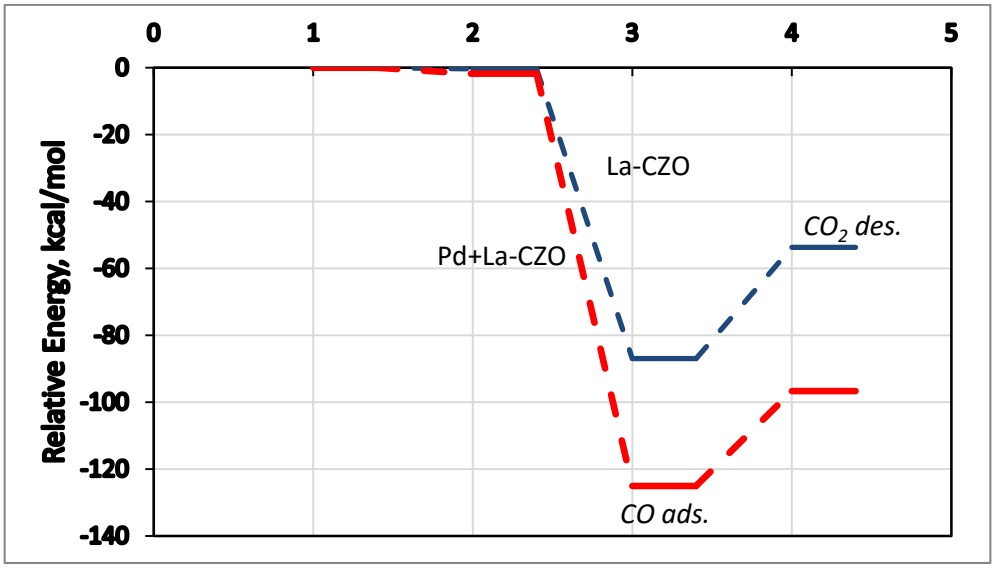

Figure 5.7 Comparison of first CO oxidation relative energies on La-CZO and Pd+La-CZO surfaces

According to CI-NEB analysis, La doped CZO surface becomes prominent compared to bimetallic substituted surface due to the lack of activation barrier at CO_2 desorption step. However, in Civan's study (2014), the synergistic effect of Pd and Mn was observed in terems of CO oxidation mechanism on Pd-surface. According to experimental studies conducting on Pd-CZO surface, La contribution enhances the NO and HC conversion while suppress the CO conversion (Wang et al., (2009, 2010, 2011); Guo et al. (2009)). On the other hand, at the La doped CeO_2 (110) surface, the interaction of CO with the surface is increased on La doped surfaces compared to the undoped surface. In this respect, in the light of findings of literature and current study, this research points out that La only doped surface may be a promising candidate for TWC.

5.3. Oxygen Vacancy Formation Energies of Surfaces

In this part, oxygen vacancy formation energies of La-$Ce_{0.75}Zr_{0.25}O_2$ and Pd-La-$Ce_{0.75}Zr_{0.25}O_2$ are investigated. For this reason, one oxygen atom is removed from the surface. Oxygen vacancy formation energy E_{vac} is calculated by the following expression

$$E_{vac} = \left(E_{vac+surface} + \frac{1}{2}E_{O_2}\right) - E_{surface} \qquad (5.1)$$

where $E_{vac+surface}$ is the energy of oxygen vacant surface, i.e. surface after CO_2 desorption; $E_{surface}$ is the energy of clean catalyst surface; E_{O_2} is the energy of oxygen molecule in the gas phase.

Oxygen vacancy formation energies of CZO catalyst surfaces with different dopant atoms are given in Table 5.3. Vacancy formation energy is calculated as 34.49 kcal/mol for La-CZO and a negative value of -4.30 kcal/mole for Pd+La-CZO surface. Oxygen vacancy formation energy on Pd-CZO (110) was computed as 43.7 kcal/mole (Gerçeker and Önal, 2013).

Incorporation of both Pd and Mn in CZO (110) surface was studied by Civan (2015). The oxygen vacancy formation energy was obtained as -12.09 kcal/mol for Mn doped Pd-CZO surface while 59.83 in the absence of Pd substitution.

Table 5.3 Oxygen vacancy formation of different CZO surfaces.

Surfaces	Oxygen Vacancy formation energy, kcal/mol
Pd-CZO (Gerceker, 2013)	43.69
La-CZO (current study)	34.49
Pd+La-CZO (current study)	-4.30
Mn-CZO (Civan, 2014)	59.83
Mn+Pd-CZO (Civan, 2014)	-12.09

As reported in Table 5.3, the lowest vacancy formation energy is of Mn+Pd doped CZO surface. It is followed by Pd+La doped CZO surface. The synergism between metal dopant and Pd atom enhances the oxygen vacancy formation of the catalyst.

CHAPTER 6

SUMMARY, CONCLUSIONS AND FUTURE WORK

In this thesis, catalytic properties of automotive exhaust emission catalysts containing Pd and Pd+La on ceria-zirconia have been investigated by quantum mechanical approach. For this reason, ceria-zirconia (110) surface was prepared and top layer of this surface is doped with atomic La and Pd+La atoms. The effect of La doping and synergetic effect of noble and rare earth metal doping were investigated in terms of catalytic activity. For this reason, CO oxidation reaction was studied on these surfaces. Concluding remarks according to the results are summarized as follows:

Since lanthanum is in the same group with cerium, its substitution on the ceria surfaces is energetically more favorable than the palladium substitution.

The formation energy of lanthanum doped CZO (110) surface is lower than that of the palladium doped CZO (110) surface. Lanthanum improves the oxygen vacancy formation property of Pd-doped surface.

CO adsorption on both lanthanum and palladium doped CZO (110) surfaces more exothermic than that of the La only doped CZO surface. It might be due to the improvement of the oxygen storage capacity of Pd+La-CZO surface as a result of a structural deformation caused by bimetallic doping.

As a result of DFT computations La doped CZO catalyst shows better performance by eliminating the activation barrier at the desorption step compared to Pd-CZO catalyst (Gerceker and Onal, 2013). In the case of bimetallic doping, desorption

step may be carried out very slow or impossible due to high activation barrier at this step. Previously conducted experimental findings reports that the light of performance of Pd-CZO catalyst is decreased by the addition of La to the catalyst. It may be explained that CO conversion is suppressed due to the activation barrier observed in the desorption step obtained in this theoretical study.

It can be concluded that surface geometry and substitutional doping play a crucial role in determining the reactivity of ceria-zirconia surfaces to the first step in CO oxidation.

As a next step of this study, the research on NOx reduction should be studied on La and Pd+La doped CZO surfaces. With the experimental knowledge that La improves the NOx reduction properties of Pd based catalyst (Wang et al, 2009), and NOx reduction should be considered on the doped CZO surfaces.

REFERENCES

Blöchl, P. E., Projector augmented-wave method. Physics Review B (1994) 50, 17953.

Born M., Oppenheimer J. R., Zur Quantentheorie der Molekeln. *Annalen der Physik* 84 (1927) 457-484.

Branda, M. M., Ferullo, R.M., Causa M., Illas F., Relative Stabilities of Low Index and Stepped CeO2 Surfaces from Hybrid and GGA+U Implementations of Density Functional Theory. *The Journal Of Physical Chemistry C* 115 (2011) 115, 3716-3721.

Chen H.T., Chang J.G., Computational Investigation of CO Adsorption and Oxidation on Iron-Modified Cerium Oxide. *J. Phys. Chem. C* 115 (2011) 14745–14753.

Civan A. , Development of Three Way Catalytic Converters for Elimination of Hydrocarbons, Carbon Monoxide and Nitric Oxide in Automotive Exhaust. *MSc Thesis*, METU (2014) Ankara.

Damyanova S., Pawelec B., Arishtirova K., Martinez Huerta M. V, Fierro J. L G, Study of the surface and redox properties of ceria-zirconia oxides. *Applied Catalysis A: General* 337:1 (2008) 86-96.

Di Monte R., Fornasiero P., Kašpar J., Graziani M., Gatica J. M., Bernal S., Gómez-Herrero A., Stabilisation of nanostructured Ce0.2Zr0.8O2 solid solution by impregnation on Al2O3: a suitable method for the production of

thermally stable oxygen storage/release promoters for three-way catalysts. *Chemical Communications* 21 (2000) 2167-2168.

Di Monte, R., Fornasiero, P., Kaspar, J., Graziani, M., Stabilisation of nanostructured CeO_2- ZrO_2 solid solutions by addition of Al_2O_3: a suitable way for production of thermally stable oxygen storage/release promoters for three-way catalysts. *Studies in Surface Science and Catalysis* 140 (2001) 229.

Di Monte R., Kaspar J., Fornasiero P., Graziani M., Pazé C., Gubitosa G., NO reduction by CO over Pd/Ce0.6Zr0.4O2.Al2O3 catalysts: in situ FT-IR studies of NO and CO adsorption. Inorg. Chimica Acta 334 (2002) 318-326.

Gandhi, H.S., Piken, A.G., Shelef, M., Delosh, R.G., Laboratory evaluation of three-way catalysts. *SAE Paper* 760201, 1976.

Gerçeker, D. and Önal, I., A DFT study on CO oxidation on Pd4and Rh4 clusters and adsorbed adsorbed Pd and Rh atoms on CeO_2 and Ce0.75Zr0.25O2 supports for TWC adsorbed Pd and Rh atoms on CeO_2 and Ce0.75Zr0.25O2 supports for TWC. *Applied Surface Science* 285 (2013) 927-936.

Guo Y., Lu G., Zhang Z., Zhang S., Liu Y.Q.Y., Preparation of (x=0.75, 0.62) solid solution and its application in Pd-only three-way catalysts. *Catalysis Today* 126 (2006) 296-302.

Heck R.M., Farrauto R.J., Automobile exhaust catalysts. *Applied Catalysis A: General* 221 (2001) 443-457.

Henkelman G., B.P. Uberuaga, and H. Jónsson, A climbing image nudged elastic band method for finding saddle points and minimum energy paths, *J. Chem. Phys.* 113 (2000) 9901.

Hohenberg P., Kohn W., Inhomogeneous electron gas. *Phys. Rev.* 136 (1964) 864–871.

Hsu L.C., Tsai M.K., Lu Y.H., Chen, H.T., Computational Investigation of CO Adsorption and Oxidation on Mn/ CeO_2 (111) Surface. *J. Phys. Chem. C* 117 (2013) 433-441.

Jensen, F., Introduction to Computational Chemistry. *John Wiley & Sons Ltd., 2nd Ed.*, 2007, England.

Kaspar J., Fornasiero P., Balducci G., Di Monte R., Hickey N., Sergo, V., Effect of ZrO2 content on textural and structural properties of CeO2-ZrO2 solid solutions made by citrate complexation route. *Inorganica Chimica Acta* 349 (2003) 217-226.

Kašpar, J.; Fornasiero, P.; Graziani, M., Use of CeO_2-based oxides in the threeway catalysis, *Catal. Today 50* (1999) 285–298.

Kašpar, J.; Fornasiero, P.; Hickey, N., Automotive catalytic converters: currentstatus and some perspectives, *Catal. Today 77* (2003) 419–449.

Kim, G., Ceria-promoted three-way catalysts for auto exhaust emission control, *Ind. Eng. Chem. Prod. Res. Dev. 21* (1982) 267–274.

Kohn W., Sham L. J., Self-consistent equations including exchange and correlation effects. *Phys. Rev. 140* (1965) 1133-1139.

Kresse, G., Furthmuller J., Efficiency of ab-inito total energy calculations for metals and semiconductors using a plane-wave basis set. *Computational Materials Science* 6 (1996) 15-50.

Kresse, G, Hafner J., Ab initio molecular dynamics simulation of the liquid-metal-amorphous-semiconductor transition in germanium. *Physical Review B 49* (1994) 14251.

Kresse G., Furthmüller J., Efficient iterative schemes for ab initio total-energy calculations using a plane-wave basis set. *Physical Review B* 54 (1996) 11169–11186.

Lassi, U., Deactivation correlations of Pd/Rh three way catalysts designed for Euro IV emission limits. Effects of ageing atmosphere, temperature and time. *Dissertation-Oulu: University of Oulu*, 2003.

Lucena, P., Vadillo, J.M., Laserna, J.J., Mapping of platinum group metals in automotive exhaust three-way catalysts using laser-induced breakdown spectrometry. Anal. Chem. 71 (1999) 4385–4391.

Li, G., Wang, Q., Zhao, B., Zhou, R., A new insight into the role of transition metals doping with CeO_2–ZrO_2 and its application in Pd-only three-way catalysts for automotive emission control. *Fuel* 92 (2012) *360-368*.

Logan, D.A.; Graham, G.W., NO chemisorption on Pd (100) with ultra-thin overlayers of oxidized La and Al, *Surf. Sci. Lett.* 277 (1992) 47–51.

Martinez-Arias, A., Conesa, J., Fernandez-Garcia, M. & Anderson, J., Supported Metals in Vehicle Emission Control. In: Supported Metals in Catalysis. *s.l.:Imperial College Press,* 2012.

Muraki, H.; Yokota, K.; Fujitani, Y., Nitric oxide reduction performance of automotive palladium catalysts. *Appl. Catal.* (1989) 48, 93–105.

Muraki, H.; Shinjoh, H.; Sobukawa, H.; Yokota, K.; Fujitani, Y., Palladium lanthanum catalysts for automotive emission control. *Ind. Eng. Chem. Prod. Res. Dev.* 25 (1986) 202–208.

Nolan, M. et al., Density functional theory studies of the structure and electronic structure of pure and defective low index surfaces of ceria. *Surface Science,* Volume 576 (2005a) 217-229.

Nolan, M., Parker, S. C. & Watson, G. W., The electronic structure of oxygen vacancy defects at the low index surfaces of ceria. *Surface Science,* Volume 595 (2005b) 223-232.

Parr R., Yang W., Density-functional theory of atoms and molecules. *Oxford University Press*, 1994, Oxford.

Perdew J. P., Chevary J. A., Vosko S. H., Jackson K. A., Pederson M. R., Singh D. J., Fiolhais C., Atoms, Molecules, Solids, and Surfaces- Applications of the Generalized Gradient Approximation for Exchange and Correlation. *Phys Rev: B* 46:11 (1992) 6671-6687.

Ramanchandran, K. I., Deepa, G., Namboori, K., Computational Chemistry and Molecular Modeling. *Springer*, 2008, Berlin.

Schrödinger E., Planck M., Einstein A., Lorentz H. A., Briefe zur Wellenmechanik. *Springer*, 1963, Berlin.

Shim, W.G., Jung, S.C., Seo, S.G., Kim, S.C., Evaluation of regeneration of spent three-way catalysts for catalytic oxidation of aromatic hydrocarbons. *Catal. Today* 164 (2011) 500–506.

Shelef, M., Graham, G.W., McCabe, R.W., Ceria and other oxygen storage components in automotive catalysts; in: Trovarelli, A. (Ed.), Catalysis by Ceria and Related Materials; *Imperial College Press Vol.2*, 2002, London.

Skoglundh, M., Johansson H., Lijwendahl L., Jansson K., Dahl L., Hirschauer, B., Cobalt-promoted palladium as a three-way catalyst. *Appl. Catal. B: Environ.* 7 (1996) 299–319.

Trovarelli, A., Catalytic Properties of Ceria and CeO2-Containing Materials. *Catalysis Reviews: Science and Engineering* 38:4 (1996) 439-520.

Twigg, M. V., Catalytic control of emissions from cars. *Catalysis Today* 163 (2011) 33-41.

Van Santen R. A., Sautet P., Computational Methods in Catalysis and Materials Science. *Wiley-VCH*, 2008, Weinheim.

Vidmar P., Fornasiero P., Kaspar J., Gubitosa G., Graziani M., Effects of Trivalent Dopants on the Redox Properties. *Journal of Catalysis* 168 (1997) 160-168.

Wang H.F., Gong. X, Guo, Y., Lu G.Z., Hu P., A Model to Understand the Oxygen Vacancy Formation in Zr- Doped CeO_2: Electrostatic Interaction and Structural Relaxation. *Journal of Physical Chemistry C* 113 (2009) 10229-10232.

Wang J., Chen H., Hu Z., Yao M., Li Y., A Review on the Pd-Based Three-Way Catalyst. *Catalysis Reviews: Science and Engineering* 57 (2015) 79–144.

Wang Q., Li G., Zhao B., Shen M., Zhou R., The effect of La doping on the structure of $Ce_{0.2}Zr_{0.8}O_2$ and the catalytic performance of its supported Pd-only three-way catalyst. *Applied Catal. B: Environ.* 101(2010) 150-159.

Wang Q., Li G., Zhao B., Zhou R., The effect of rare earth modification on ceria-zirconia solid solution and its application in Pd-only three-way catalyst. *J. of Molecular Catalysis A: Chemical* 339 (2011) 52-60.

Wang Q., Zhao B., Li G., Zhou R., Application of Rare Earth Modified Zr-based Ceria-Zirconia Solid Solution in Three-Way Catalyst for Automotive Emission Control. *Environ. Sci. Technol.* 44 (2010) 3870-3875).

Yang, Z., Lu, Z., Luo G., Hermansson, K., Oxygen vacancy formation energy at the Pd/CeO_2 (111) interface. *Physics Letters A* 369 (2007) 132-139.

Yeriskin I., Nolan M., Doping of ceria surfaces with lanthanum: a DFT+ ***U*** study. *J. Phys.: Condens. Matter* 22 (2010) 135004.

Yeriskin I., Nolan M., Effect of La doping on CO adsorption at ceria surfaces. *J. Chem. Phys.* 131 (2009) 244702-(1-6).

Zhao B., Li G., Ge C., Wang Q., Zhou R., Preparation of $Ce_{0.67}Zr_{0.33}O_2$ mixed oxides as supports of improved Pd-only three-way catalysts. *Applied Catalysis B: Environmental* 96 (2010) 338-349.

Zhao B., Wang Q, Li G., Zhou R., Effect of rare earth (La, Nd, Pr, Sm and Y) on the performance of Pd/ $Ce_{0.67}Zr_{0.33}MO_{2-x}$ three-way catalyst. *J. Environmental Chem. Eng.* 1 (2013) 534-543.

APPENDICES

APPENDIX A

SAMPLE INPUT FILES FOR VASP CODE

A.1. Sample VASP Bodes for Bulk Optimization

A.1.1. INCAR FILE

```
SYSTEM = CeO2
!ISTART = 0
PREC = HIGH
ISIF = 3
IBRION = 1;
NSW = 150
LREAL = AUTO
ISMEAR = 0; SIGMA = 0.01;
ENCUT = 500
ALGO = FAST
EDIFFG = -0.001
```

A.1.2. KPOINTS FILE

```
K-Points
 0
Monkhorst Pack
 18 18 18
 0 0 0
```

A.2. Sample VASP Codes for Surface Optimizations

A.2.1. INCAR File

```
EDIFFG = -0.015

IBRION = 2
!POTIM = 0.2;
!NFREE  = 20



ISMEAR = 0; SIGMA = 0.01;
LREAL = Auto
ENCUT  = 500
IDIPOL = 3

LDIPOL = .TRUE.
NSW    = 300

ALGO=FAST
```

A.2.2. KPOINTS File

```
K-Points
 0
Monkhorst Pack
 4 4 1
 0 0 0
```

A.3. Sample VASP Codes for CI-NEB Calculations

A.3.1. INCAR File

```
!FOR CI-NEB
IMAGES = 8
SPRING = -5
ICHAIN = 0
LCLIMB = .TRUE.
LTANGENTOLD = .FALSE.
LDNEB  = .FALSE.
!EDIFFG = -0.015

IBRION = 1;
POTIM = 0.2;
!NFREE  = 20

NSW    = 500
LDIPOL = .TRUE.

ISMEAR = 0; SIGMA = 0.1;
LREAL = Auto
ENCUT  = 500
IDIPOL = 3



LCHARG = .FALSE.
ALGO=FAST
```

A.3.2. KPOINTS File

```
K-Points
 0
Monkhorst Pack
 4 4 1
 0 0 0
```